



OPEN

Pyrazole derivatives of pyridine and naphthyridine as proapoptotic agents in cervical and breast cancer cells

Rima D. Alharthy¹, Faisal Rashid², Abida Ashraf³, Zahid Shafiq^{4,5}, Steven Ford⁶, Mariya al-Rashida⁷, Muhammad Yaqub⁴ & Jamshed Iqbal²✉

Cancer is one of the leading causes of death worldwide. The increasing prevalence and resistance to chemotherapy is responsible for driving the search of novel molecules to combat this disease. In search of novel compounds with pro-apoptotic potential, pyrazolo-pyridine and pyrazolo-naphthyridine derivatives were investigated against cervical cancer (HeLa) and breast cancer (MCF-7) cells. The anti-proliferative activity was determined through the MTT assay. Potent compounds were then analyzed for their cytotoxic and apoptotic activity through a lactate dehydrogenase assay and fluorescence microscopy after propidium iodide and DAPI staining. Flow cytometry was used to determine cell cycle arrest in treated cells and pro-apoptotic effect was verified through measurement of mitochondrial membrane potential and activation of caspases. Compounds 5j and 5k were found to be most active against HeLa and MCF-7 cells, respectively. G0/G1 cell cycle arrest was observed in treated cancer cells. Morphological features of apoptosis were also confirmed, and an increased oxidative stress indicated the involvement of reactive oxygen species in apoptosis. The compound-DNA interaction studies demonstrated an intercalative mode of binding and the comet assay confirmed the DNA damaging effects. Finally, potent compounds demonstrated a decrease in mitochondrial membrane potential and increased levels of activated caspase-9 and -3/7 confirmed the induction of apoptosis in treated HeLa and MCF-7 cells. The present work concludes that the active compounds 5j and 5k may be used as lead candidates for the development of lead drug molecules against cervical and breast cancer.

Cancer is a multi-factorial disease which is characterized by unchecked and abnormal cellular division of poorly differentiated cells. Tumorigenesis is a complex multistage process in which a group of cells, in a specific part of the body, starts unlimited replication due to genetic and epigenetic modifications^{1,2}. Tumorigenesis involves an initiation step in which mutations in a cell population drive the cells to unchecked replication by by-passing apoptotic signals. Heterogeneity is observed in such cell clusters. Such cells produce larger populations, start affecting nearby cells, enlarge their size and consequently invade to other body parts or systems, a characteristic of malignancy known as metastasis³. Benign tumors are devoid of invasive nature due to sac like covering around them produced by the body's defense mechanisms and they remain non-invasive unless a major mutational change induces malignancy. Benign tumors are easy to handle and can be effectively treated through conventional therapy, however, malignancy is life threatening. If a tumor is metastatic, it requires rigorous treatment, intensive care and critical monitoring of untoward effects⁴.

Cancer can be life threatening if not diagnosed and treated in the earlier stages. Oncological treatments include surgical removal of the developed cancer lump, radiation therapy, hormonal starvation therapy for certain

¹Chemistry Department, Faculty of Science and Arts, King Abdulaziz University, Rabigh 21911, Saudi Arabia. ²Centre for Advanced Drug Research, COMSATS University Islamabad, Abbottabad Campus, Abbottabad 22060, Pakistan. ³Department of Chemistry, Kutchery Campus, The Women University Multan, Multan 60000, Pakistan. ⁴Institute of Chemical Sciences, Bahauddin Zakariya University, Multan, Pakistan. ⁵Department of Pharmaceutical and Medicinal Chemistry, University of Bonn, An der Immenburg 4, 53121 Bonn, Germany. ⁶Department of Pharmaceutical Sciences, Institute of Pharmacy and Biomedical Sciences, University of Strathclyde, Glasgow, UK. ⁷Department of Chemistry, Forman Christian College (A Chartered University), Lahore, Pakistan. ✉email: jamshediqb@googlemail.com

cancers, immunotherapy by sensitizing cancer cells to the immune system and boosting its efficiency, stem cell transplants specially for non-solid tumors, genetic sequencing for identifying the genetic causes of a cancer and by chemotherapeutics to induce apoptosis in cancer cells⁵.

Dealing with multi-factorial and complex diseases is a big challenge and polychemotherapy or polypharmacy is facing problems: specifically patient non-compliance and resistance to chemotherapy. In synthetic pharmaceutical chemistry, “multi-target directed ligand” approach is an emerging strategy in which two or more pluripotent pharmacophores are hybridized into a single molecule to augment a therapeutic effect through multiple actions on a target^{6–8}. Molecular hybridization is very promising in minimizing side effects⁹, facilitating access to target organs¹⁰ and making hybrid molecules resistant to resistance development^{11–13}. Consequently, hybrid-drug designing is making an overall improvement in current therapeutics regarding efficacy, selectivity and safety.

Hybridizing two or more active pharmacophores to achieve better outcomes in disease management is now a regular practice. Pyrazolo-pyridine derivatives have been shown to be antimalarial, antiviral, anti-leishmanial, anti-tubercular, anti-leukemic, antifungal, anxiolytic, osteogenic and have antitumor activity. Moreover, they have also been studied in management of drug and alcohol addiction, Alzheimer’s disease, infertility and gastrointestinal diseases¹⁴. Mohamed et al.¹⁵ synthesized pyrazolo-cyanopyridine derivatives having antitumor activity. Pyrazolo pyrimidine and pyridine derivatives were synthesized and tested against human laryngeal epidermoid carcinoma (HEp2) cells¹⁶. Two of the investigated compounds showed good antitumor activity. The compounds were also investigated on four cancer cell lines and all except one, were found to be potent against breast, hepatic, prostate and colon cancer cells¹⁷. Some novel pyrazolo pyridine derivatives were investigated for their anticancer activity in liver, colon and breast carcinoma cells, and all compounds were found to be antiproliferative agents¹⁸. Pyrazolopyridine derivatives also depicted good anticancer potential¹⁹. Thienopyridine and pyrazolopyridine derivatives showed good anti-proliferative activity in colon, liver and breast cancer cells²⁰.

Naphthyridine derivatives have been reported as antifungal²¹, anticancer²², antibacterial²³, GSK-3 inhibitors²⁴, trypanocidal²⁵, insecticidal²⁶ acetyl and butyryl-cholinesterase inhibitors^{27,28}. Their anticancer effect was previously studied by various research groups. A number of pyrazolo-naphthyridin derivatives showed noteworthy antiproliferative activity²⁹. Similarly 1,8-naphthyridine derivatives, also showed good antitumor activity with IC₅₀ values ranging from 1.47 to 35.3 μ M in breast cancer cells³⁰. These studies prompted us to investigate pyrazolo-pyridine (**4a–4n**) and pyrazolo-naphthyridine (**5a–5n**) for their potential to be used as antiproliferative agents.

Results

Anti-proliferative activity and structure activity relationship (SAR). In search of new anti-neoplastic agents, the anti-proliferative potential of pyrazolopyridines (**4a–4n**) and pyrazolonaphthyridines (**5a–5n**) against MCF-7 and HeLa cells was evaluated by testing each compound at 100 μ M. Non-cancerous BHK-21 cells were used to evaluate cytotoxicity of these compounds. Anti-proliferative potential was calculated as percentage of inhibition (% inhibition) and are shown in Table 1. The IC₅₀ values were calculated and shown in Table 2. Compounds **5j** and **5k** were found to be the most active compounds with IC₅₀ values of 6.4 ± 0.45 and 2.03 ± 0.23 μ M against HeLa and MCF-7 cells respectively. Among twenty eight tested compounds, fourteen were found active against HeLa and MCF-7 cells. Compound **5j** was the most active against HeLa, whereas, then compound **5k** was the most active against MCF-7 cells (see Table 2).

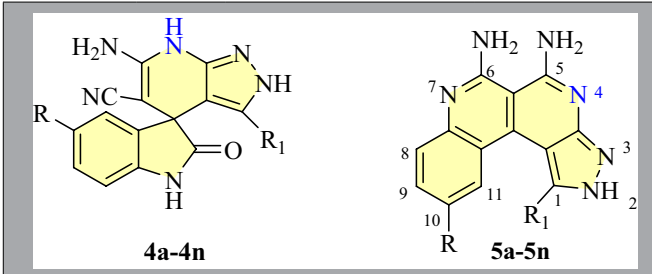
Cytotoxic activity. The cytotoxic activity of active compounds **5j** and **5k** was determined by estimation of cytosolic lactate dehydrogenase (LDH) enzyme. A dose dependent increase in leaked LDH was measured in HeLa and MCF-7 cells after treatment with compounds **5j** and **5k** (Fig. 1) which showed good cytotoxic potential of potent compounds in these cells.

Cytotoxicity, apoptosis and ROS determination by fluorescence microscopy. Nuclear staining dyes propidium iodide (PI) and 4',6-diamidino-2-phenylindole (DAPI) were used to identify cytotoxic and apoptotic effect of the most active compound **5j** and **5k**. Cell population decreased as dead cells became non-adherent while some apoptotic cells remained attached and were stained by PI and DAPI. Cell detachment, shrinkage of cells and condensation of nuclear material was observed [Fig. 2 (a–f, j–o)] in a dose dependent manner after treatment with compound **5j** and **5k**.

The production of ROS in treated cells was estimated by 2',7'-dichlorodihydrofluorescein diacetate (H₂DCF-DA) staining which showed an intense green fluorescence in treated cells as compared to control class as shown in Fig. 2 (g–i, p–r).

Analysis of cell cycle by flow cytometry. The DNA content measurement in each phase of cell cycle was evaluated through flow cytometry after PI staining of compound **5j** treated cells and compared with untreated control cells. Compound **5j** showed G₀/G₁ arrest in HeLa cells (Fig. 3).

Determination of compound-DNA interactions. The interaction of potent compound **5j** with DNA was studied: hypochromicity for two chromophores was observed with no red or blue shift, which indicated that compound **5j** was non-covalently bound to DNA. A Gibbs free energy of $\Delta G = -14$ kJ/mol was calculated for this reaction. Absorption spectra has been shown in Fig. 4. The compound-DNA interaction was further verified by in silico studies. Figure 5 shows the docked conformation of most active compound **5j** against DNA, exhibiting an intercalator binding mode (as expected due to the rigid planar rings of the molecule).



Code	R	R ₁	HeLa cell line	MCF-7 cell line
			%Inhibition at 100 μM	
4a	H	H	34.53	28.17
4b	CH ₃	H	45.87	1.86
4c	F	H	57.80	26.82
4d	Cl	H	99.45	18.88
4e	Br	H	24.91	7.24
4f	NO ₂	H	26.17	5.23
4g	OCF ₃	H	38.64	15.23
4h	H	CH ₃	5.08	2.38
4i	CH ₃	CH ₃	39.67	1.42
4j	F	CH ₃	5.68	2.22
4k	Cl	CH ₃	3.84	11.90
4l	Br	CH ₃	39.31	1.78
4m	NO ₂	CH ₃	22.67	23.33
4n	OCF ₃	CH ₃	27.81	0.15
5a	H	H	97.91	46.36
5b	CH ₃	H	98.40	96.36
5c	F	H	69.25	4.12
5d	Cl	H	71.40	27.27
5e	Br	H	98.30	96.81
5f	NO ₂	H	26.99	9.54
5g	OCF ₃	H	61.30	31.36
5h	H	CH ₃	93.60	37.83
5i	CH ₃	CH ₃	63.50	58.18
5j	F	CH ₃	94.80	47.83
5k	Cl	CH ₃	96.40	69.50
5l	Br	CH ₃	81.60	28.18
5m	NO ₂	CH ₃	44.91	10.33
5n	OCF ₃	CH ₃	63.16	10.47
Cisplatin	-	-	98.63	73.12

Table 1. Anti-proliferative activity of pyrazolopyridine and pyrazolonaphthyridine derivatives against HeLa and MCF-7 cells.

Determination of DNA damage by comet assay. The cervical cancer (HeLa) cells were treated with 6.4 μM of compound 5j. Cells treated for 30 min with 20 μM of freshly prepared H₂O₂ were used as positive control. Images were captured as shown in Fig. 6 and analyzed by ImageJ and OpenComet. DNA damage was assessed by calculating the comet parameters tail length, %DNA in tail and tail moment as shown in Table 3 and Fig. 7. Compound 5j showed DNA damage in treated cells, comparable to positive control.

Measurement of mitochondrial membrane potential ($\Delta\Psi_m$). The cationic dye JC-1 was utilized to evaluate MMP in HeLa and MCF-7 cells after treatment with potent compounds 5j and 5k at their IC₅₀ and 2 × IC₅₀ values. A decrease in red/green ratio was observed in both HeLa and MCF-7 cells which indicated that the compounds caused a decrease in the mitochondrial membrane potential. The effect was comparatively less in HeLa cells as compared to MCF-7 cells as shown in Fig. 8.

Determination of activated caspase-9 and caspase-3/7. The compounds 5j and 5k were selected for carrying out assays of caspase activation in HeLa and MCF-7 cells respectively. An increase of 1.4 and 2.2-folds

Code	HeLa Cell Line	MCF-7 cell line	BHK-21 cell line
	IC ₅₀ (μM) ± SEM		
4c	90.21 ± 2.18	–	49.21 ± 2.01
4d	51.63 ± 0.99	–	246.41 ± 6.71
5a	58.91 ± 0.39	–	177.42 ± 6.11
5b	32.12 ± 1.14	41.35 ± 0.47	126.23 ± 1.63
5c	10.31 ± 0.51	–	42.41 ± 1.95
5d	40.72 ± 1.42	–	166.81 ± 0.95
5e	30.23 ± 1.15	18.61 ± 0.29	84.11 ± 3.31
5f	69.11 ± 0.99	–	100.83 ± 2.61
5h	14.42 ± 1.21	–	31.42 ± 1.33
5i	61.93 ± 1.76	54.68 ± 0.63	133.91 ± 1.71
5j	6.43 ± 0.45	–	27.51 ± 1.32
5k	7.25 ± 0.12	2.03 ± 0.23	8.21 ± 0.57
5l	38.51 ± 0.63	–	151.62 ± 2.61
5n	32.73 ± 2.16	–	46.61 ± 1.03
Cisplatin	11.33 ± 0.78	6.22 ± 0.72	24.69 ± 0.37

Table 2. IC₅₀ values of the most active pyrazolo-pyridine (4a–4n) and pyrazolo-naphthyridine (5a–5n) derivatives. SEM standard error of mean.

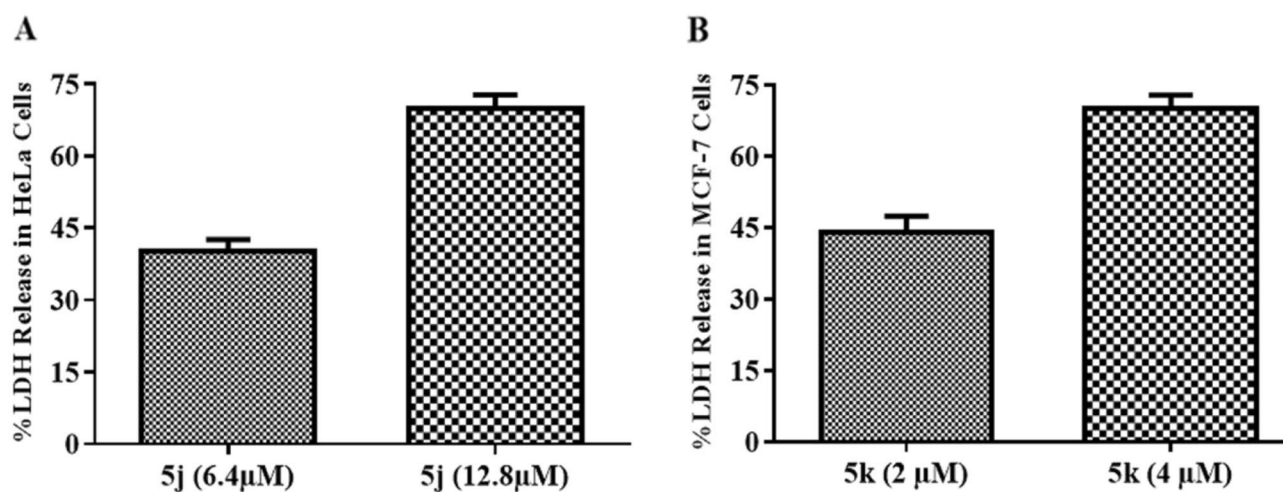


Figure 1. Cytotoxic effect of compounds 5j and 5k observed in (A) HeLa and (B) MCF-7 cells respectively by estimation of released LDH. Error bars represent standard deviation of three replicates.

was observed for activated caspase-9 while about 4 and 4.8-folds increase in activated caspase-3/7 was observed in HeLa cells treated at IC₅₀ and 2 × IC₅₀ values of compound 5j, respectively. A fold increase of 1.1 and 1.4-folds in activated caspase-9 whereas, 1.4 and 1.8-fold increases in activated caspase-7 was observed in MCF-7 cells treated with compound 5k at IC₅₀ and 2 × IC₅₀ values, respectively (Fig. 9).

Discussion

The MTT assay is the most commonly used high throughput method to screen potential anti-proliferative compounds and is based on the reduction of a water soluble, yellow dye, MTT, to water insoluble, purple colored formazan crystals by the action of oxidoreductases present in healthy cells³¹. In present study, compounds 5j and 5k were found to be the most active compounds with IC₅₀ values of 6.4 ± 0.45 and 2.03 ± 0.23 μM against HeLa and MCF-7 cells respectively. The structure activity relationship was determined based on the anti-proliferative effects observed in the MTT cell viability assay. In case of pyrazolopyridines (4a–4n), an H atom was present at position R₁ (4a–4g). When an H atom was at R₁, a mild increase in anti-proliferative activity was observed in HeLa cells. Only two compounds (4c, 4d) showed good anticancer activity (i.e., having > 50% inhibition at 100 μM) when R₁ was an H-atom and R was one of two strongly electronegative halogen atoms. When H atom at R₁ was replaced by methyl group (4h–4n), a decrease in anti-proliferative activity was observed when there were either H or less bulky electronegative atoms like –F and –Cl groups at R₁ (4h, 4j and 4k). A mild increase

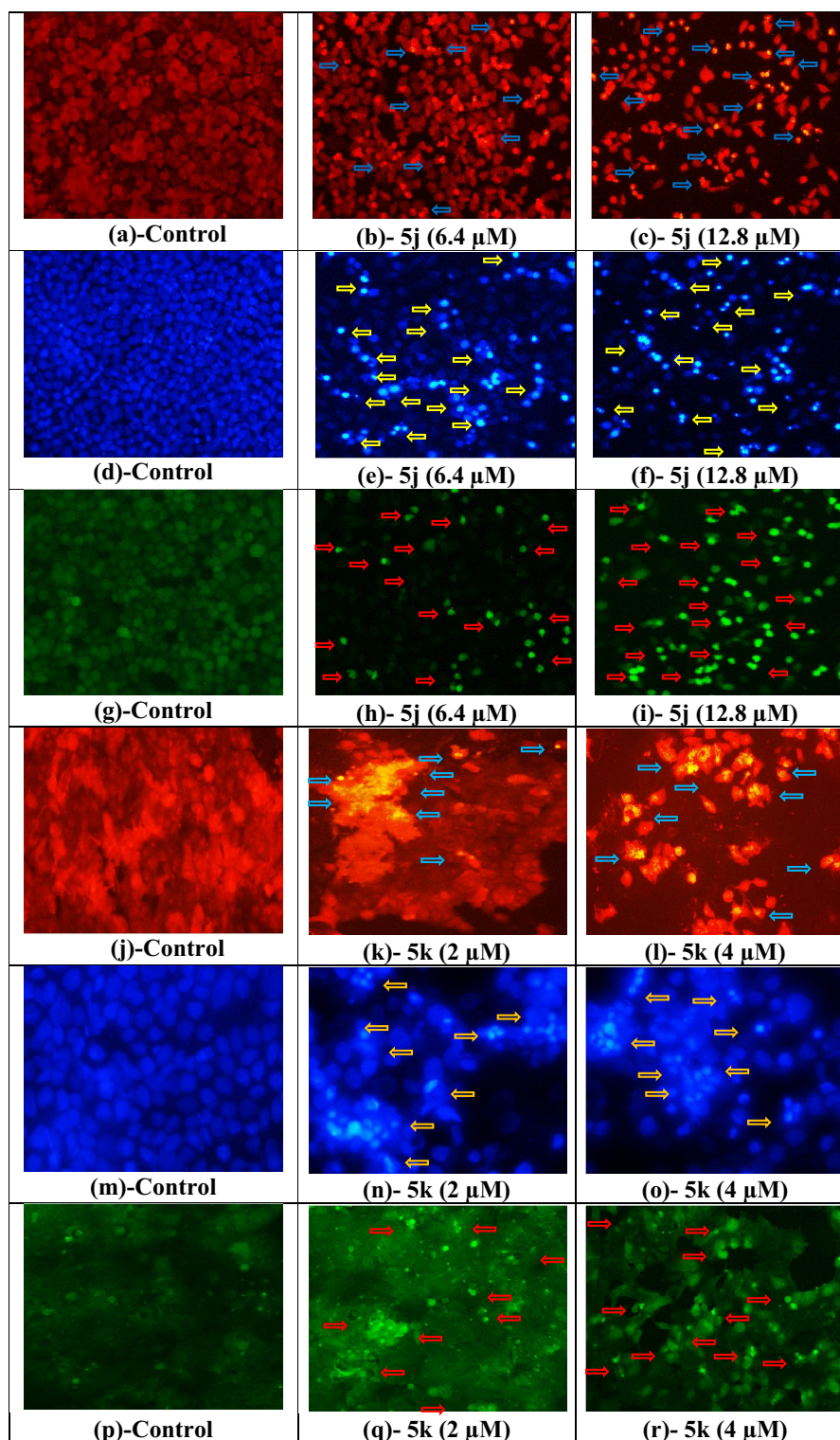


Figure 2. Fluorescence photomicrographs of untreated, compound **5j** treated HeLa cells after PI (a–c), DAPI (d–f) and H₂DCF-DA (g–i) staining and compound **5k** treated MCF-7 cells after PI (j–l), DAPI (m,n,o) and H₂DCF-DA (p–r) staining. Images are showing dose dependent cytotoxic, apoptotic and ROS generation indicated by arrows in compound **5j** treated HeLa and **5k** treated MCF-7 cells as compared to control.

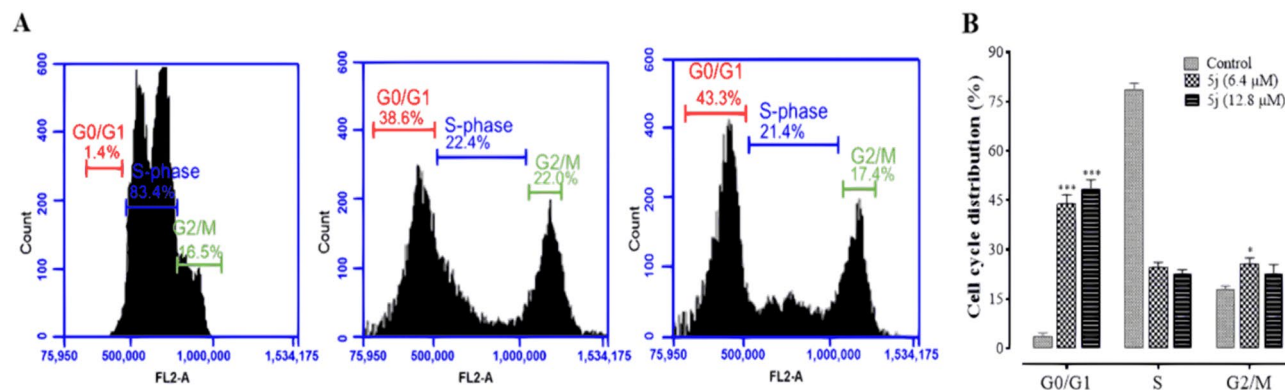


Figure 3. Compound 5j induced cell cycle arrest. (A) The representative results of cell cycle analysis obtained by flow cytometry in untreated (control) and compound 5j treated cells. (B) The proportions of G0/G1, S and G2/M phases are represented as mean \pm SD. * $p < 0.05$, ** $p < 0.01$, *** $p < 0.001$ versus control group ($n = 3$).

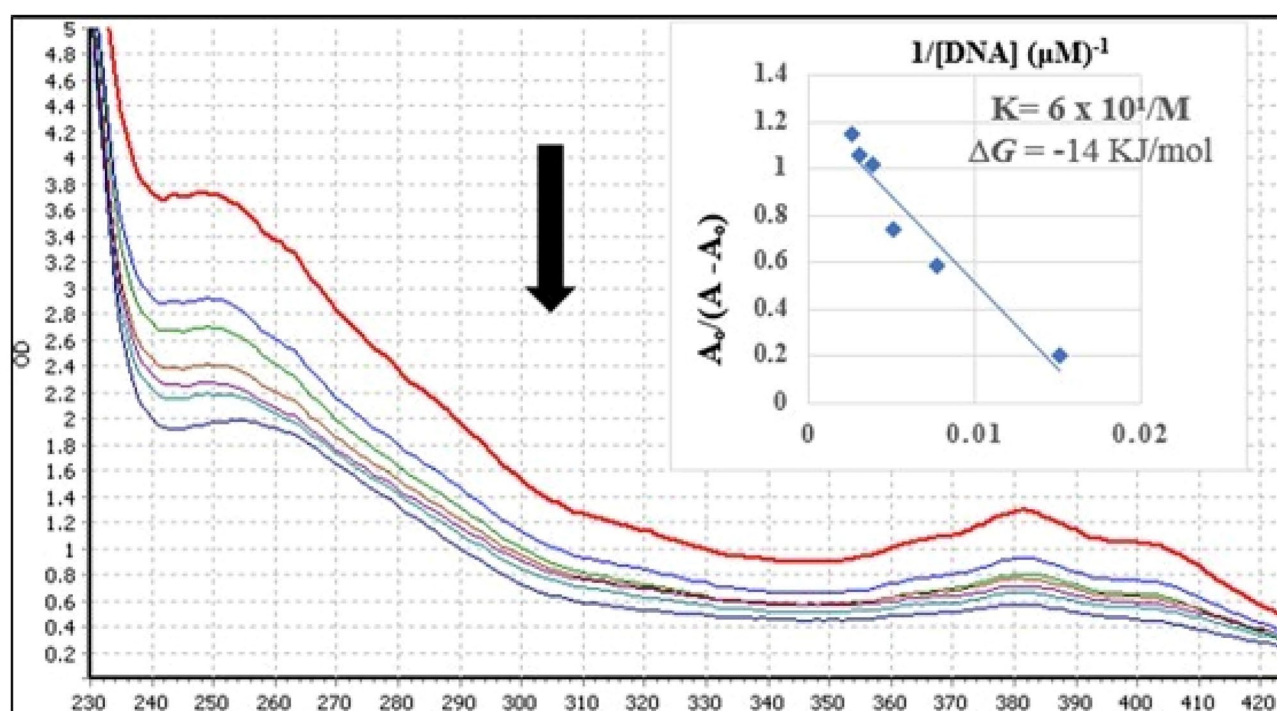


Figure 4. Absorption spectra of 200 μM of 5j in absence (0 μM) and presence (66, 132, 198, 264, 330 and 396 μM) of DNA. The arrow direction shows increasing concentration of DNA. The graph is the plot of $A_0/(A - A_0)$ versus $1/[DNA]$ for the determination of binding constant and Gibbs's free energy of 5j-DNA product.

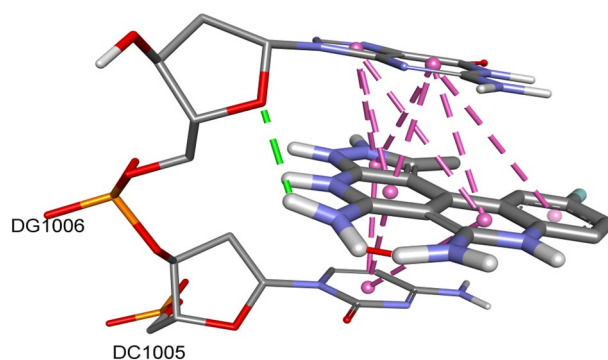


Figure 5. Docked conformation of DNA, compound 5j.

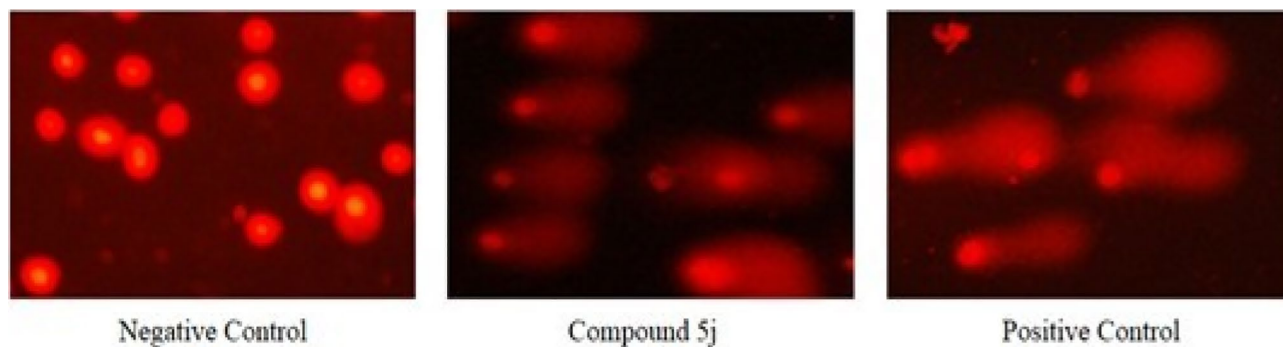


Figure 6. Representative images of comets obtained from untreated, compound **5j** treated and H_2O_2 treated HeLa cells by alkaline comet assay to assess DNA damage.

Sample	Tail length \pm SD (μM)	%DNA in tail \pm SD	Tail moment \pm SD
5j	43.01 \pm 10.27	41.02 \pm 7.61	23.22 \pm 1.61
Untreated	9.91 \pm 4.36	19.65 \pm 5.33	6.47 \pm 2.51
H_2O_2	84.14 \pm 3.43	55.11 \pm 0.68	3.37

Table 3. DNA damage parameters calculated for compound **5j**, untreated and H_2O_2 treated cells. *SD* standard deviation.

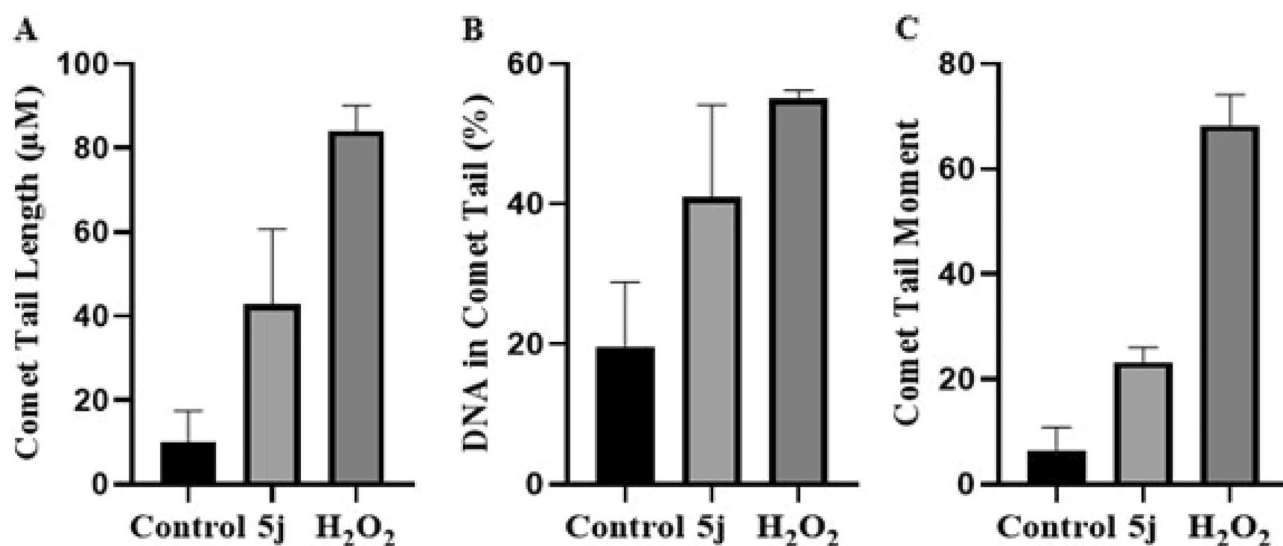


Figure 7. Quantitative analysis of (A) comet tail length, (B) percent DNA in tail and (C) comet tail moment in untreated, compound **5j** treated and H_2O_2 treated cells. Data are represented as mean \pm SD in replicate of three. * $p < 0.05$, ** $p < 0.01$, *** $p < 0.001$ versus control group ($n = 3$).

in activity was observed when the position R was a $-\text{CH}_3$ group (**4i**) or bulky electronegative atom or groups like $-\text{Br}$, $-\text{NO}_2$, $-\text{OCF}_3$ (**4l**, **4m** and **4n**).

In case of pyrazolonaphthyridines (**5a–5n**), all compounds were found active except two compounds (**5f** and **5m**). The H atom was kept constant at R_1 and substitutions were made at R (**5a–5g**). When the H atom was present at R (**5a**), an increase in anti-proliferative activity was noticed which further increased when H atom at R was replaced by $-\text{CH}_3$ (**5b**) group. Substitution of $-\text{NO}_2$ group (**5f**) yielded the least active compound which exhibited an inhibition of less than 50%. Bromo substitution (**5e**) yielded more active compound as compared to chloro (**5d**) substitution. However, replacing halogens with $-\text{NO}_2$ (**5f**) group yielded least active compound among these derivatives against HeLa cells. Activity was increased when $-\text{NO}_2$ was replaced by $-\text{OCF}_3$ group (**5g**) in both cancer cell lines. Among seven derivatives (**5h–5n**), when R_1 was a methyl group ($-\text{CH}_3$), fluoro substitution at R yielded the most active compound (**5j**) in HeLa cells. Anti-proliferative activity was dependent on strength of electronegativity (**5j** > **5k** > **5l**) against HeLa cells. Substitution of $-\text{NO}_2$ (**5m**) caused a decrease in activity. Substitution of $-\text{NO}_2$ did not yield active compounds. The anti-proliferative potential of these compounds was attributed to the presence of halogen atoms at R position of benzene ring attached to naphthyridine ring.

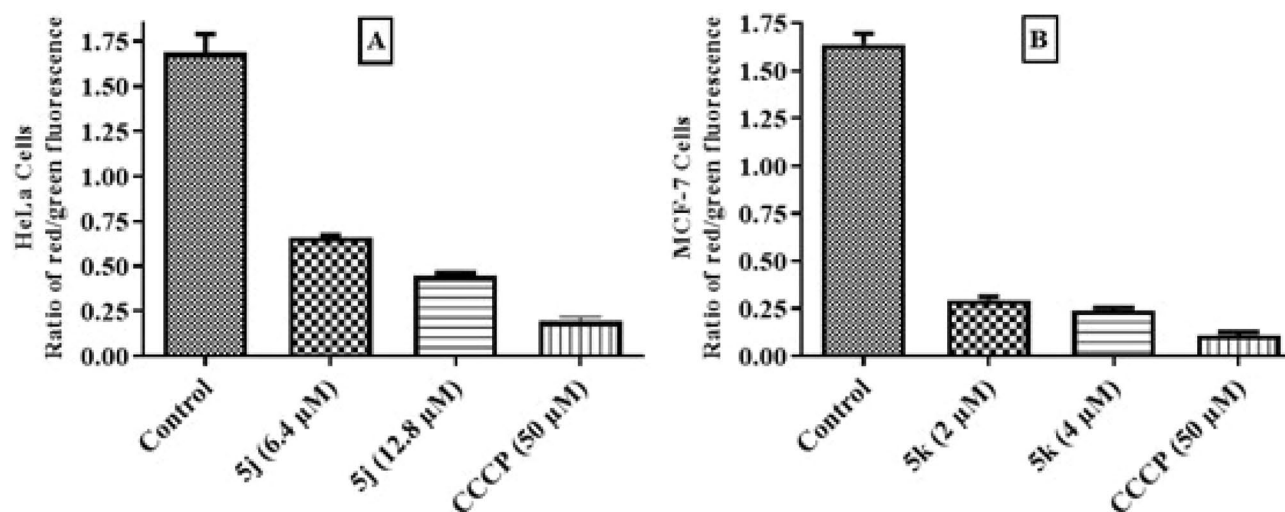


Figure 8. Quantitative analysis of depolarization of mitochondrial membrane potential in compounds **5j** and **5k** treated cells by observing ratio of red/green fluorescence after JC-1 staining. The untreated (control) cells maintained normal $\Delta\Psi_m$ while treated cells are showing compromised $\Delta\Psi_m$. Data are represented as mean \pm SD in replicate of three. * $p < 0.05$, ** $p < 0.01$, *** $p < 0.001$ versus control group ($n = 3$).

Further mechanistic studies were designed to evaluate possible mechanism of action of the most active compounds at fairly effective doses. As the number of cells was high in these assays as compared to MTT assay so IC_{50} and $2 \times IC_{50}$ values, calculated in MTT assay, were chosen in order to have a significant number of cells at the end of experiment against each dose. LDH assay is a reliable method to determine the cytotoxic potential of a test compound in cells. This assay is based on the fact that dying cells possess a highly permeable membrane as compared to live cells. Cellular contents can leak out of this permeable membrane. The LDH is a cytosolic enzyme which is responsible for interconversion of pyruvate and lactate during glycolysis^{32,33}. At end of apoptosis, when cells have a permeable or ruptured membrane, the LDH that leaks out of cell is measured and the cytotoxicity of the test compound calculated with respect to positive and negative control. The treatment of cells with compounds **5j** and **5k** showed an increase in leaked LDH which depicted that these compounds have a sound cytotoxic potential against cancer cells.

Apoptotic and dying cells have a permeable cell membrane. Cell impermeable molecules can easily enter through permeable membranes. Fluorescence microscopy has made it possible to visualize apoptotic features in cells using fluorescence probes. Nuclear staining dyes propidium iodide (PI) and 4',6-diamidino-2-phenylindole (DAPI) selectively enter in apoptotic cells and cross nuclear membrane where upon binding to DNA, their fluorescence increases manifold. Cell detachment, shrinkage of cells and condensation of nuclear material was increased in a dose dependent fashion after treatment with compounds **5j** and **5k** which depicted that potent compounds have potential to induce apoptosis in cancer cells.

Reactive oxygen species (ROS) were considered as byproducts of metabolism but with the passage of time their role in cell signaling was also discovered. They both are equally essential to healthy cells, as well as toxic, inducing different metabolic diseases and even apoptosis depending upon their level of production. At low levels, they are involved in cell signaling pathways while at higher levels, they are toxic to cells^{34,35}. High oxidative stress triggers apoptosis in cancer cells^{36,37}. A dose dependent ROS generation in treated cells may be attributed to dysfunctioning of mitochondria which may lead to apoptosis via a mitochondrial pathway³⁸. Our results were in compliance with a published study³⁹.

The cell cycle is a highly regulated and organized cellular process that occurs in parallel to apoptosis to maintain homeostasis. In cancer cells, the cell cycle process becomes continuous and uncontrolled due to mutational changes in regulating genes. Anticancer agents trap this cell cycle and can cause an arrest in this process at any stage, ultimately pushing these cells to apoptosis. Cyclin-CDK (cyclin dependent kinases) complexes are the main cell cycle regulatory proteins which may be down-regulated due to interactions with anti-proliferative agents. DNA content varies in different phases of the cell cycle which can be detected in the cells using fluorescent probes through flow cytometry. Compound **5j** showed G0/G1 arrest in HeLa cells that may be attributed to inhibition of cyclin D-CDK 4 and cyclin E-CDK 2 complex⁴⁰.

Most anticancer agents target DNA and the interactions with DNA produce their apoptotic effect. The interaction of potent compound **5j** with DNA was studied: hypochromicity for two chromophores was observed with no red or blue shift, which indicated that compound **5j** was non-covalently bound to DNA. The docked conformation of **5j** against DNA exhibited an intercalation binding mode (as expected due to the rigid planar rings of the molecule). A hydrogen bond was observed between the ring oxygen atom of guanine nucleic acid base and the amino group. A number of hydrophobic pi-pi stacked interactions were observed between bases G and C with the aromatic rings of **5j**. The observed intercalative interaction was due to pi-pi stacked interactions of aromatic rings of **5j** with DNA bases and is in compliance with a published study³⁰. Moreover, compound **5j**

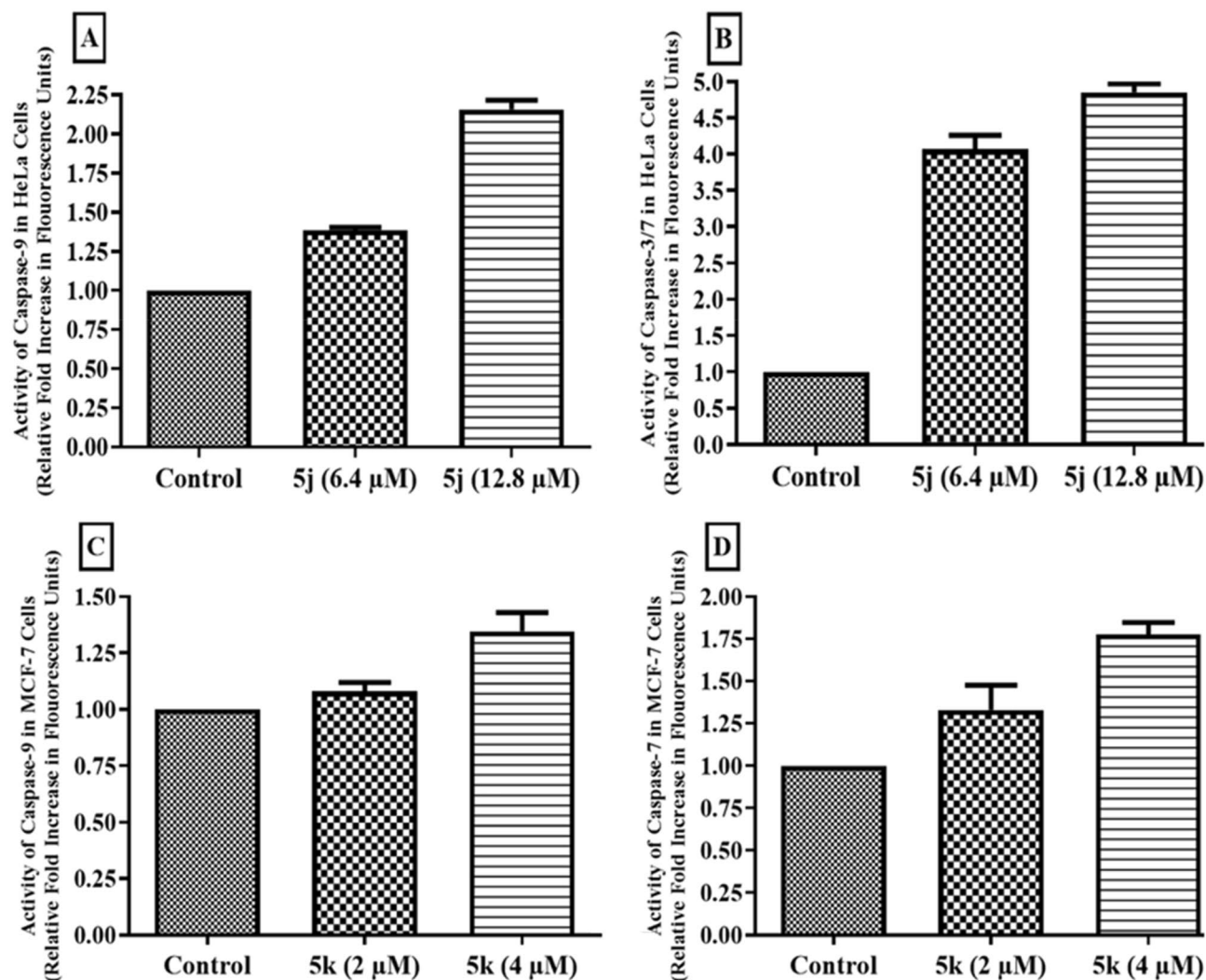


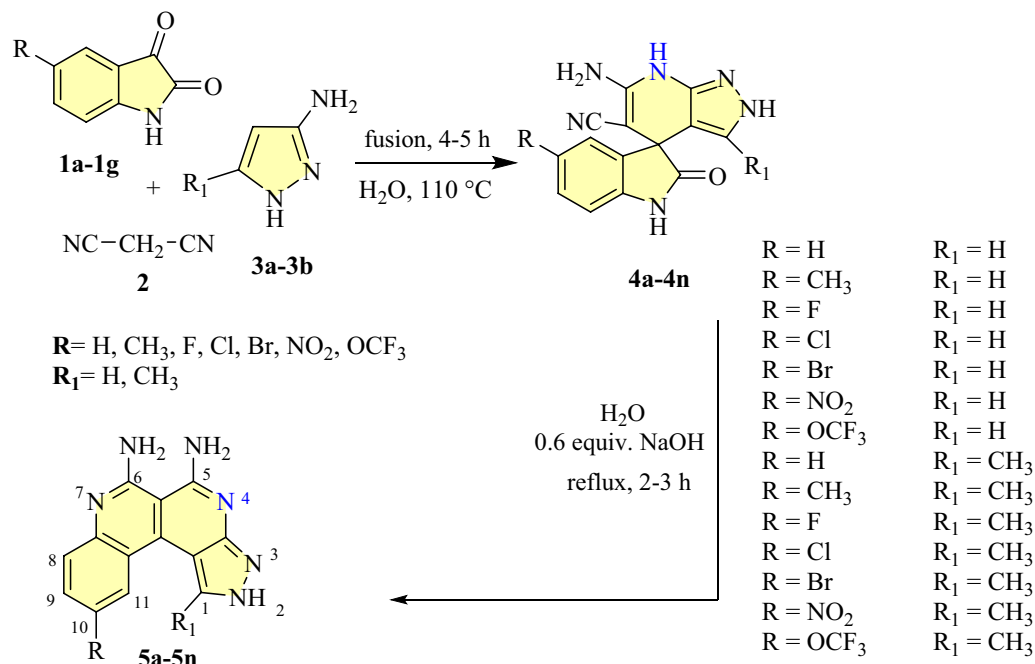
Figure 9. Fold increase in activity of (A) caspase-9 and (B) caspase-3/7 in HeLa cells after treatment with compound 5j. Fold increase in (C) caspase-9 and (D) caspase-7 in MCF-7 cells after treatment with compound 5k. Data are represented as mean \pm SD in replicate of three. * $p < 0.05$, ** $p < 0.01$, *** $p < 0.001$ versus control group ($n = 3$).

showed DNA damage in treated cells which revealed that the compound binds to DNA and causes DNA damage to induce apoptosis.

Mitochondria are important organelles in cells which manage cellular energy needs. Mitochondrial membrane has a relatively high negative charge as compared to cell membrane. Some apoptotic agents may cause damage to the mitochondrial membrane and consequently lead to a decrease in mitochondrial membrane potential (MMP). Increased mitochondrial membrane permeability leads to release of cytochrome c which combines with Apaf-1 (apoptotic protease activating factor 1) to form apoptosome that consequently activate caspases which ultimately executes the process of apoptosis⁴¹. Compounds 5j and 5k caused a dose dependent decrease in MMP which was in compliance with a published study⁴².

Caspases are enzymes which are mostly activated in the apoptotic cascade. They are non-functional or down-regulated in cancer cells due to mutational changes. These enzymes are proteolytic in their functionality and make the cells non-functional due to the loss of essential proteins during an apoptotic cascade. Caspase-9 is activated due to the formation of apoptosome which activates executioner caspases-3/7. Compounds 5j and 5k caused an increase in activated caspases in treated HeLa and MCF-7 cells respectively and confirming their apoptotic potential against cancer cells. Our findings were in compliance with a previous study³⁹.

Pyrazolo pyridine derivatives (4a–4n) were found, in general, to be less active than cisplatin with only two active compounds (4c and 4d) showing higher IC_{50} values than cisplatin. Pyrazolo-naphthyridines were highly active against cervical cancer (HeLa) and breast cancer (MCF-7) cells except compound 5f and 5m. Compounds 5j and 5k were the most active compounds inducing apoptosis in HeLa and MCF-7 cells at micromolar concentrations. The cytotoxic potential against cancer cells for both compounds was confirmed through LDH assay. A G0/G1 cell cycle arrest, higher cytotoxic and apoptotic potential observed through fluorescence microscopy using PI and DAPI staining, an increased oxidative stress confirmed by H_2DCF -DA staining, intercalative binding



Scheme 1. Preparation of pyrazolo-pyridine (**4a–4n**) derivatives and pyrazolo-naphthyridine (**5a–5n**) derivatives⁴³.

with DNA and DNA damaging effects in treated cancer cells represented the pro-apoptotic activity of most active compounds. The potent compounds (**5j** and **5k**) also induced a decrease in mitochondrial membrane potential and an increase in activated caspases in treated HeLa and MCF-7 cells, both are indicative of the activation of the mitochondrial pathway of apoptosis induced by these compounds in cancer cells. Conclusively, the potent compounds (**5j** and **5k**) can be used as lead candidates for the development of drug against cervical and breast cancers.

Materials and method

Materials. All the chemicals used for the synthesis of naphthyridine derivatives, were purchased from Sigma-Aldrich. Lyophilized Herring sperm DNA, 3-(4,5-dimethylthiazolyl-2)-2,5-diphenyltetrazolium bromide (MTT, Lot# MKBQ2167V), propidium iodide (PI, Lot# SLBH8362V), 4',6'-diamidino-2-phenylindole (DAPI, Lot# 034M4030V), 2',7'-dichlorodihydrofluorescein diacetate (H₂DCF-DA) and 5',5',6',6'-tetrachloro-1',1',3',3'-iodide (JC-1, Lot# MKBR2378V) dyes, agarose (Low gelling temp.).

CCCP (Carbonyl cyanide *m*-chlorophenyl hydrazone) were purchased from Sigma Aldrich, USA. Cell culture components RPMI (Roswell Park Memorial Institute Medium, Lot # 688600), DMEM (Dulbecco's modified Eagles Medium, Lot# 02150011), fetal bovine serum (FBS, Lot # 2440071), trypsin-EDTA (Lot# 2259320) and penicillin streptomycin (Pen/Strep, Lot# 2321148) were purchased from Gibco, USA. Phosphate buffered saline (PBS) tablets, RNase A, and agarose from Invitrogen, USA, Triton X-100 from AppliChem, Germany and formaldehyde (37%) from Scharlau, Spain, H₂O₂ (Hydrogen Peroxide) (30%) from Thermo-Fisher Scientific, dimethyl sulfoxide DMSO (sterile) from DAEJUNG, Korea, Albumin Fraction V (Bovine Serum Albumin, BSA) from Carl Roth GmbH & Co. Kg, Germany were also used in biological assays.

Breast cancer (MCF-7, ATCC[®] HTB-22[™]), cervical cancer (HeLa, ATCC[®] CCL-2[™]) and Baby Hamster kidney (BHK-21, ATCC[®] CCL-10[™]) cells were gifted by Dr. Syed Shahzad ul Hussan from Lahore University of Management Sciences (LUMS), Lahore, Pakistan. Main stocks of these cells were cryopreserved at -196 °C. MCF-7 cells were grown in DMEM supplemented with 15% FBS and 1% Pen/Strep while HeLa and BHK-21 cells were grown in RPMI supplemented with 10% FBS and 1% Pen/Strep.

Synthesis of synthesis of pyrazolo-pyridine (4a–4n**) and pyrazolo-naphthyridine (**5a–5n**) derivatives.** The synthesis of spiro pyrazolo-pyridine (**4a–4n**) and pyrazolo-naphthyridine (**5a–5n**) derivatives were carried out by following the Scheme 1 as reported previously⁴³.

MTT cell viability assay. The anti-proliferative activity of the studied compounds was determined against breast (MCF-7) and cervical (HeLa) cancer cells by the MTT cell viability assay as described earlier^{44,45}. BHK-21 cells were used as non-cancerous cells to study the effect of these compounds on normal cells. Briefly, 1×10^4 cells/well were seeded in 96-well microtiter plate and placed in an incubator (Heracell[™] VIOS 160i, Thermo-Fisher Scientific) set for 5% CO₂ at 37 °C. The stock solutions of compounds were prepared at 10 mM concentration in DMSO. Initial working solutions were prepared in cell culture medium at 1 mM concentration. Compounds exhibiting more than 50% inhibition at 100 μM end concentration were further tested at lower concentrations

(100 to 2.5 μM) to calculate IC_{50} values. After 24 h, medium in each well was aspirated and cells were treated for 4 h with serum free medium containing 0.2 mg/mL MTT reagent. The solubilizing reagent (10% acidified sodium dodecyl sulfate in propanol in a 1:1 ratio) was added to solubilize formazan crystals. Plates were kept at 37 °C for 30 min and then placed on a gyratory shaker for few min for complete solubilization of formazan crystals. The optical density was measured at 570 nm by microplate reader and IC_{50} values were calculated from three independent experiments as previously reported⁴⁶.

LDH cytotoxicity assay. The cytotoxic potential of the most active compounds was evaluated by measuring the lactate dehydrogenase released into cell culture medium by compound-treated cells using the Pierce LDH Cytotoxicity Assay Kit (Lot# SF252000, Thermo Scientific). Briefly, 1×10^4 cells/well were seeded in a flat bottom 96 well cell culture plate and kept for overnight incubation. Cells were treated with potent compounds **5j** and **5k** at the IC_{50} and $2 \times \text{IC}_{50}$ values. The plate was centrifuged at 1500 rpm for 3 min and the supernatant (50 μL) transferred to a new sterile 96-well plate. After addition of substrate mix (50 μL), plate was placed at room temperature for 30 min. The absorbance was measured at 490 nm and 680 nm using microplate reader (FLUOstar Omega, Ortenberg, Germany). Cytotoxicity was measured as described earlier⁴⁷.

Microscopic analysis of apoptosis. Morphological changes in compound treated cancer cells were identified using propidium iodide (PI) and 4',6-diamidino-2-phenylindole (DAPI) staining with observing under a fluorescence microscope (Nikon ECLIPSE Ni-U, Japan). Briefly, 2×10^5 cells/well were grown on microscopic slides and treated with IC_{50} and $2 \times \text{IC}_{50}$ values of the most active compounds **5j** and **5k**. After 24 h, media was aspirated, cells were washed with sterile phosphate buffered saline (PBS) and fixed by using 4% formalin and 0.1% Triton X-100 as adherent cells fixation solution. Further, 10 μL (0.01 mg/mL) of PI or DAPI solution was added on slides and kept for 10 min in dark. Fluorescence photomicrographs were captured as previously reported⁴⁸.

Determination of oxidative stress. The potential of most active compound to induce apoptosis in treated cancer cells via production of reactive oxygen species was analyzed by fluorescence microscope (Nikon ECLIPSE Ni-U, Japan) after 2',7'-dichlorodihydrofluorescein diacetate ($\text{H}_2\text{DCF-DA}$) staining. Cells (2×10^5) grown on microscopic slides were treated with IC_{50} and $2 \times \text{IC}_{50}$ values of the most active compounds **5j** and **5k**. After washing with sterile PBS, cells were fixed and 10 μL (0.01 mg/mL) of $\text{H}_2\text{DCF-DA}$ dye was added on microscopic slides. After an incubation of 10 min at room temperature in the dark, fluorescence photomicrographs were obtained as previously reported⁴⁹.

Cell cycle analysis assay. The variation in cell cycle distribution was observed in cancer cells treated with potent compound **5j** by flow cytometer (BD Accuri™ C6, USA). Briefly, HeLa cells (2×10^5 cells/mL) were grown and treated with IC_{50} and $2 \times \text{IC}_{50}$ values of potent compound **5j**. Cells were harvested and washed three times with PBS to remove traces of cell culture medium. Cells were fixed in 70% ethanol for 24 h at -20 °C. Pelletized cells were then re-suspended in 1 mL of a solution containing PI (20 $\mu\text{g/mL}$), RNase A (50 $\mu\text{g/mL}$) and 0.1% (v/v) Triton X-100. Samples were kept in the dark for 30 min at room temperature and analyzed within an hour as reported earlier⁵⁰.

DNA binding studies. The interaction of the most active compound **5j** with herring sperm DNA was performed following a published methodology^{48,51}. A stock solution of 5 mg of DNA was prepared in 10 mL of distilled water and the purity of the DNA (A_{260}/A_{280}) was in the range of 1.6 to 1.9. Compound **5j** was tested at a final concentration of 200 μM with varying end concentrations (0 to 396 μM) of DNA. The plate was placed at room temperature for 30 min and the UV absorption spectrum was recorded by microplate reader (FLUOstar Omega BMG Labtech, Ortenberg, Germany).

DNA docking studies. For DNA-docking studies, the crystal structure of DNA was downloaded from the PDB (PDB id: 1kci). AutoDock Vina was used for the docking studies. The docking method was first validated by re-docking the co-crystallized ligand, the software was able to give the same conformation (<2 Å rmsd) of the ligand as seen in the crystal structure.

Comet assay. Comet assay is a sensitive method to determine DNA damage which was performed after some modifications in a published protocol⁵². DNA binding and molecular docking studies suggested intercalation of compound with DNA, so a single dose (IC_{50} value) was sufficient to validate these findings by evaluating DNA damage through comet assay. The cervical cancer (HeLa) cells were treated with IC_{50} value of potent compound **5j** for 24 h. Cells were harvested, collected and centrifuged to obtain a pellet. Pelleted cells were re-suspended in media. Untreated cells were used as control cells. For the positive control, 2×10^4 cells were treated with 20 μM of freshly prepared hydrogen peroxide for 30 min. Slides were prepared by coating with 1% normal melting point agarose (NMPA) on one side and then dried. Samples (2×10^4 cells/sample) were re-suspended in 1 mL of PBS. In a tube, 0.4 mL cell suspension was mixed with 1.2 mL of 0.9% low melting point agarose (LMPA) and mixed thoroughly by pipetting. A cell suspension of 65 μL was laid on coated slide and evenly distributed by placing a coverslip over it. Slides were placed at -20 °C for 10 min. Then the slides were placed at 4 °C in the dark in a lysis buffer of 100 mM EDTA, 10 mM Trizma base, 2.5 M sodium chloride, 10% DMSO and 1% Triton X-100 in distilled water with a pH of 10. After an overnight incubation, slides were washed with chilled distilled water. These slides were then placed in electrophoresis chamber (Wealtec, USA) having chilled (4 °C) alkali unwinding

solution (300 mM sodium hydroxide and 1 mM EDTA in distilled water). Electrophoresis was carried out at an adjusted voltage (between 0.7 and 1.0 V/cm) for 35 min in an electrophoresis tank. Slides were then immersed in neutralization solution (0.4 M Trizma base in 800 mL water, pH 7.5) for 10 min in dark. Propidium iodide (20 μ L of 0.01 mg/mL) was used as fluorescent dye to stain DNA. Slides were placed in dark at room temperature. After 10 min, images were captured using a fluorescence microscope (Nikon ECLIPSE Ni-U, Japan) at an excitation/emission wavelength of 493/632 nm. Microscopic images were analyzed using ImageJ (ij152-win-java8, National Institutes of Health, Bethesda, USA) and OpenComet (OpenComet_imagej_v1.3.1, USA) where the DNA content in the head and tail of the comets were automatically measured by the software. Results of three independent experiments were expressed as tail length (μ M), %DNA in comet tail and comet tail moment.

Measurement of mitochondrial membrane potential ($\Delta\Psi$ m). Mitochondrial membrane potential was determined by a fluorimetric method using fluorescent dye 5',5',6',6'-tetrachloro-1',1',3',3'-iodide (JC-1). Briefly, 1×10^5 cells were grown and treated with IC_{50} and $2 \times IC_{50}$ values of compounds **5j** and **5k** for 24 h. Cells were harvested, pelletized and treated with 0.25 μ M of fluorescent dye JC-1. Each sample was transferred to a flat-bottomed black 96-well plate, which was kept in the dark for 20 min. Fluorescence emission was measured by a fluorescent microplate reader (FLUOstar Omega BMG Labtech, Germany) at 590 nm and 520 nm for j-aggregates and j-monomers. Results were measured as ratio of red/green fluorescence as previously reported⁵³.

Apoptosis assessment by caspase -9 and -3/7 activity. Activation of apoptosis inducing caspases were determined using fluorimetric assay kits by Abcam (ab65607 (Lot# GR3194417-1) & ab39383 (Lot# GR3188949-1)). Briefly, 1×10^6 cells were grown and treated with IC_{50} and $2 \times IC_{50}$ values of potent compounds **5j** and **5k**. Cells were harvested after 18 h treatment and washed with PBS. Pelletized cells were treated with lysis solution and the lysate transferred to new eppendorf tubes. After protein quantification using "Total Protein Biuret (Lot# 210-B) Kit", the lysate was treated with substrates of caspase-9 and caspase-3/7 in a black 96-well plate. Fluorescence excitation/emission at 400/505 nm was measured by fluorescence microplate reader (Bio-Tek FLx800™, Instrument, Inc. USA). Results were represented as fold increase in activated caspase-9 and caspase-3/7 as compared to control as previously reported⁴⁶.

Statistical analysis. The data was presented as the mean \pm SEM or mean \pm SD of at least three independent experiments. Statistical analyses were performed using Student's t-test and graphs were drawn by GraphPad Prism (version 8.0.2). Values of $p \leq 0.05$ were considered statistically significant.

Data availability

The datasets used and/or analysed during the current study available from the corresponding author on reasonable request.

Received: 6 October 2022; Accepted: 28 March 2023

Published online: 01 April 2023

References

- Jones, P. A. & Baylin, S. B. The epigenomics of cancer. *Cell* **128**, 683–692 (2007).
- Chanock, S. J. The paradox of mutations and cancer. *Science* **362**, 893–894 (2018).
- Tabassum, D. P. & Polyak, K. Tumorigenesis: It takes a village. *Nat. Rev. Cancer* **15**, 473–483 (2015).
- Kim, Y. J., Siegler, E. L., Siriwon, N. & Wang, P. Therapeutic strategies for targeting cancer stem cells. *J. Cancer Metastasis Treat.* **2**, 233–242 (2016).
- Miller, K. D. *et al.* Cancer treatment and survivorship statistics, 2016. *CA Cancer J. Clin.* **66**, 271–289 (2016).
- Meunier, B. Hybrid molecules with a dual mode of action: Dream or reality?. *Acc. Chem. Res.* **41**, 69–77 (2008).
- Teiten, M.-H., Dicato, M. & Diederich, M. Hybrid curcumin compounds: A new strategy for cancer treatment. *Molecules* **19**, 20839–20863 (2014).
- Noh, J. *et al.* Amplification of oxidative stress by a dual stimuli-responsive hybrid drug enhances cancer cell death. *Nat. Commun.* **6**, 1–9 (2015).
- Gediya, L. K. & Njar, V. C. Promise and challenges in drug discovery and development of hybrid anticancer drugs. *Expert Opin. Drug Discov.* **4**, 1099–1111 (2009).
- Oh, J.-M. *et al.* Efficient delivery of anticancer drug MTX through MTX-LDH nanohybrid system. *J. Phys. Chem. Solids* **67**, 1024–1027 (2006).
- Marco-Contelles, J. & Soriano, E. The medicinal chemistry of hybrid-based drugs targeting multiple sites of action. *Curr. Top. Med. Chem.* **11**, 2714–2715 (2011).
- Zhang, Z., Bi, C., Fan, Y., Wang, H. & Bao, Y. Cefepime, a fourth-generation cephalosporin, in complex with manganese, inhibits proteasome activity and induces the apoptosis of human breast cancer cells. *Int. J. Mol. Med.* **36**, 1143–1150 (2015).
- Punganuru, S. R., Madala, H. R. & Srivenugopal, K. S. Colchicine-based hybrid anticancer drugs to combat tumor heterogeneity. *Med. Chem.* **6**, 165–173 (2016).
- Samar, C., Ismail, A., Helmi, T., Khiari, J. & Bassem, J. Substituted pyrazolo [3,4-b] pyridin-3-ones and pyrazolo [3,4-b] pyridine-5-carbaldehyde, new one-pot synthesis strategy amelioration using vinamidinium salts, antibacterial and antifungal activities promising environmental protection. *J. Bacteriol. Parasitol.* <https://doi.org/10.4172/2155-9597.1000310> (2017).
- Mohamed, M. S., Awad, Y.E.E.-D., El-Hallouty, S. M. & El-Araby, M. Design, synthesis and cancer cell line activities of pyrazolo [3,4-b] pyridine derivatives. *Open J. Med. Chem.* **2**, 78–88 (2012).
- Abdel-Latif, E., Abdel-Fattah, S., Gaffer, H. E. & Etman, H. A. Synthesis and antitumor activity of some new pyrazolo [3,4-d] pyrimidine and pyrazolo [3,4-b] pyridine derivatives. *Egypt. J. Basic Appl. Sci.* **3**, 118–124 (2016).
- Eissa, I. H., El-Naggar, A. M. & El-Hashash, M. A. Design, synthesis, molecular modeling and biological evaluation of novel 1H-pyrazolo [3,4-b] pyridine derivatives as potential anticancer agents. *Bioorg. Chem.* **67**, 43–56. <https://doi.org/10.1016/j.bioorg.2016.05.006> (2016).
- Metwally, N. H. & Deeb, E. A. Synthesis, anticancer assessment on human breast, liver and colon carcinoma cell lines and molecular modeling study using novel pyrazolo [4,3-c] pyridine derivatives. *Bioorg. Chem.* **77**, 203–214 (2018).

19. Chavva, K. *et al.* Synthesis and biological evaluation of novel alkyl amide functionalized trifluoromethyl substituted pyrazolo [3,4-b] pyridine derivatives as potential anticancer agents. *Bioorg. Med. Chem. Lett.* **23**, 5893–5895 (2013).
20. Elneairy, M. A. A., Eldine, S. M. & Mohamed, A. S. I. Novel fused thienopyridine and pyrazolopyridine derivatives: Synthesis, characterization and cytotoxicity. *Der. Pharma Chem.* **7**, 284–295 (2015).
21. Abdelrazek, F. M., Kassab, N. A.-L., Metwally, N. H. & Sobhy, N. A. Synthesis of some novel pyridine and naphthyridine derivatives. *Eur. J. Chem.* **1**, 368–372 (2010).
22. Hassaneen, H. M., Wardkhan, W. W. & Mohammed, Y. S. A novel route to isoquinoline [2,1-g][1,6] naphthyridine, pyrazolo [5,1-a] isoquinoline and pyridazino [4',5': 3,4] pyrazolo [5,1-a] isoquinoline derivatives with evaluation of antitumor activities. *Zeitschrift für Naturforschung. B J. Chem. Sci.* **68**, 895–904 (2013).
23. Makhanya, T. R., Gengan, R. M. & Ata, A. Synthesis and biological evaluation of novel fused indolo [3,2-c][1,8] naphthyridine derivatives as potential antibacterial agents. *Synth. Commun.* **46**, 823–835 (2019).
24. Arlan, F. M., Khalafy, J. & Maleki, R. One-pot three-component synthesis of a series of 4-aryloxy-1,6-diaryl-3-methyl-1H-pyrazolo [3,4-b] pyridine-5-carbonitriles in the presence of aluminum oxide as a nanocatalyst. *Chem. Heterocycl. Compd.* **54**, 51–57 (2018).
25. Elkholy, Y. M. An efficient synthesis of pyrazolo [3,4-b] quinolin-3-amine and benzo [b][1,8] naphthyridine derivatives. *Molecules* **12**, 361–372 (2007).
26. Hou, Q.-Q., Jing, Y.-F. & Shao, X.-S. Synthesis and insecticidal activities of 1,8-naphthyridine derivatives. *Chin. Chem. Lett.* **28**, 1723–1726 (2017).
27. Barreiro, E. J. *et al.* Design, synthesis, and pharmacological profile of novel fused pyrazolo [4,3-d] pyridine and pyrazolo [3,4-b] [1,8] naphthyridine isosteres: A new class of potent and selective acetylcholinesterase inhibitors. *J. Med. Chem.* **46**, 1144–1152 (2003).
28. Silva, D. *et al.* Synthesis and pharmacological assessment of diversely substituted pyrazolo [3,4-b] quinoline, and benzo [b] pyrazolo [4,3-g][1,8] naphthyridine derivatives. *Eur. J. Med. Chem.* **46**, 4676–4681 (2011).
29. Acosta, P. *et al.* Microwave-assisted synthesis of novel pyrazolo [3,4-g][1,8] naphthyridin-5-amine with potential antifungal and antitumor activity. *Molecules* **20**, 8499–8520 (2015).
30. Al-romaizan, A. N., Jaber, T. S. & Ahmed, N. S. Novel 1,8-naphthyridine derivatives: Design, synthesis and in vitro screening of their cytotoxic activity against MCF7 cell line. *Open Chem.* **17**, 943–954 (2019).
31. Berridge, M. V., Herst, P. M. & Tan, A. S. Tetrazolium dyes as tools in cell biology: New insights into their cellular reduction. *Biotechnol. Annu. Rev.* **11**, 127–152 (2005).
32. Legrand, C. *et al.* Lactate dehydrogenase (LDH) activity of the number of dead cells in the medium of cultured eukaryotic cells as marker. *J. Biotechnol.* **25**, 231–243 (1992).
33. Wolterbeek, H. T. & Meer, A. J. V. D. Optimization, application, and interpretation of lactate dehydrogenase measurements in microwell determination of cell number and toxicity. *Assay Drug Dev. Technol.* **3**, 675–682 (2005).
34. Pereira, E. J., Smolko, C. M. & Janes, K. A. Computational models of reactive oxygen species as metabolic byproducts and signal-transduction modulators. *Front. Pharmacol.* **7**, 1–9 (2016).
35. Forrester, S. J., Kikuchi, D. S., Hernandez, M. S., Xu, Q. & Griendling, K. K. Reactive oxygen species in metabolic and inflammatory signaling. *Circ. Res.* **122**, 877–902 (2018).
36. Kannan, K. & Jain, S. K. Oxidative stress and apoptosis. *Pathophysiology* **7**, 153–163 (2000).
37. Redza-Dutordoir, M. & Averill-Bates, D. A. Activation of apoptosis signalling pathways by reactive oxygen species. *Biochim. Biophys. Acta Mol. Cell Res.* **1863**, 2977–2992 (2016).
38. Miceli, M. V., Jiang, J. C., Tiwari, A., Rodriguez-Quinones, J. F. & Jazwinski, S. M. Loss of mitochondrial membrane potential triggers the retrograde response extending yeast replicative lifespan. *Front. Genet.* **2**, 1–11 (2012).
39. Kim, S. H. *et al.* MHY-449, a novel dihydrobenzofuro [4,5-b][1,8] naphthyridin-6-one derivative, mediates oxidative stress-induced apoptosis in AGS human gastric cancer cells. *Oncol. Rep.* **34**, 288–294 (2015).
40. Jiang, Y., Wang, X. & Hu, D. Furanodienone induces G0/G1 arrest and causes apoptosis via the ROS/MAPKs-mediated caspase-dependent pathway in human colorectal cancer cells: A study in vitro and in vivo. *Cell Death Dis.* **8**, 1–14 (2017).
41. Ricci, J.-E. *et al.* Disruption of mitochondrial function during apoptosis is mediated by caspase cleavage of the p75 subunit of complex I of the electron transport chain. *Cell* **117**, 773–786 (2004).
42. Capozzi, A. *et al.* A new 4-phenyl-1,8-naphthyridine derivative affects carcinoma cell proliferation by impairing cell cycle progression and inducing apoptosis. *Anticancer Agents Med. Chem.* **12**, 653–662 (2012).
43. Ashraf, A., Shafiq, Z., Mahmood, K., Yaqub, M. & Rauf, W. Regioselective, one-pot, multi-component, green synthesis of substituted benzo [c] pyrazolo [2,7] naphthyridines. *RSC Adv.* **10**, 5938–5950 (2020).
44. Mosmann, T. Rapid colorimetric assay for cellular growth and survival: Application to proliferation and cytotoxicity assays. *J. Immunol. Methods* **65**, 55–63 (1983).
45. Niks, M. & Otto, M. Towards an optimized MTT assay. *J. Immunol. Methods* **130**, 149–151 (1990).
46. Uddin, N. *et al.* Synthesis, characterization, and anticancer activity of Schiff bases. *J. Biomol. Struct. Dyn.* **38**, 3246–3259 (2020).
47. Scifo, C. *et al.* Resveratrol and propolis as necrosis or apoptosis inducers in human prostate carcinoma cells. *Oncol. Res. Featur. Preclin. Clin. Cancer Ther.* **14**, 415–426 (2004).
48. Iqbal, J., Ejaz, S. A., Saeed, A. & Al-Rashida, M. Detailed investigation of anticancer activity of sulfamoyl benz (sulfon) amides and 1H-pyrazol-4-yl benzamides: An experimental and computational study. *Eur. J. Pharmacol.* **832**, 11–24 (2018).
49. Shah, H. S., Joshi, S. A., Haider, A., Kortz, U. & Iqbal, J. Synthesis of chitosan-coated polyoxometalate nanoparticles against cancer and its metastasis. *RSC Adv.* **5**, 93234–93242 (2015).
50. Hamdani, S. S. *et al.* Cytotoxicity, pro-apoptotic activity and in silico studies of dithiocarbamates and their structure based design and SAR Studies. *Med. Chem.* **15**, 892–902 (2019).
51. Sirajuddin, M., Ali, S., Shah, N. A., Khan, M. R. & Tahir, M. N. Synthesis, characterization, biological screenings and interaction with calf thymus DNA of a novel azomethine 3-((3,5-dimethylphenylimino) methyl) benzene-1,2-diol. *Spectrochim. Acta Part A Mol. Biomol. Spectrosc.* **94**, 134–142 (2012).
52. Olive, P. L. & Banáth, J. P. The comet assay: A method to measure DNA damage in individual cells. *Nat. Protoc.* **1**, 23–29 (2006).
53. Al-anbaky, Q. *et al.* Cytotoxicity of manganese (III) complex in human breast adenocarcinoma cell line is mediated by the generation of reactive oxygen species followed by mitochondrial damage. *Int. J. Toxicol.* **35**, 672–682 (2016).

Acknowledgements

The authors are thankful to the Deanship of Scientific Research, King Abdulaziz University, Jeddah, Saudi Arabia (G: 328-363-1436) for great support of this work.

Author contributions

J.I. designed the project. Z.S. and M.Y. provided the synthesized compounds. F.R. and A.A. performed the experiments and wrote the manuscript. M.A. and S.F. reviewed the manuscript. R.D.A. analyse the data and supported chemicals and funding.

Competing interests

The authors declare no competing interests.

Additional information

Correspondence and requests for materials should be addressed to J.I.

Reprints and permissions information is available at www.nature.com/reprints.

Publisher's note Springer Nature remains neutral with regard to jurisdictional claims in published maps and institutional affiliations.



Open Access This article is licensed under a Creative Commons Attribution 4.0 International License, which permits use, sharing, adaptation, distribution and reproduction in any medium or format, as long as you give appropriate credit to the original author(s) and the source, provide a link to the Creative Commons licence, and indicate if changes were made. The images or other third party material in this article are included in the article's Creative Commons licence, unless indicated otherwise in a credit line to the material. If material is not included in the article's Creative Commons licence and your intended use is not permitted by statutory regulation or exceeds the permitted use, you will need to obtain permission directly from the copyright holder. To view a copy of this licence, visit <http://creativecommons.org/licenses/by/4.0/>.

© The Author(s) 2023